Phase Transitions of the Coupled Membrane-Cytoskeleton Modify Cellular Shape

Alex Veksler and Nir S. Gov
Department of Chemical Physics, The Weizmann Institute of Science, Rehovot, Israel

ABSTRACT Formation of protrusions and protein segregation on the membrane is of a great importance for the functioning of the living cell. This is most evident in recent experiments that show the effects of the mechanical properties of the surrounding substrate on cell morphology. We propose a mechanism for the formation of membrane protrusions and protein phase separation, which may lay behind this effect. In our model, the fluid cell membrane has a mobile but constant population of proteins with a convex spontaneous curvature. Our basic assumption is that these membrane proteins represent small adhesion complexes, and also include proteins that activate actin polymerization. Such a continuum model couples the membrane and protein dynamics, including cell-substrate adhesion and protrusive actin force. Linear stability analysis shows that sufficiently strong adhesion energy and actin polymerization force can bring about phase separation of the membrane protein and the appearance of protrusions. Specifically, this occurs when the spontaneous curvature and aggregation potential alone (passive system) do not cause phase separation. Finite-size patterns may appear in the regime where the spontaneous curvature energy is a strong factor. Different instability characteristics are calculated for the various regimes, and are compared to various types of observed protrusions and phase separations, both in living cells and in artificial model systems. A number of testable predictions are proposed.

INTRODUCTION

Membrane protrusions built of actin filaments (1) are of a great importance both for the functioning of the living cell (microvilli in intestinal cells, stereocilia in the inner ear cells, neuronal dendrites, etc.), and for the cell motility (lamellipodia and filopodia). Phase separation of membrane components such as proteins, lipids, and cholesterol, i.e., the formation of aggregates (rafts) on the cell membrane, is also an important process that determines cell behavior (2,3). It has been found experimentally that these two phenomena may be closely related in many circumstances in living cells, where the membrane region, deformed by the protrusion, has a very different composition compared to flat regions (see, for example, (4,5)). This relation of composition to membrane curvature has also been demonstrated recently in a simple in vitro model system (6), and in a model system that contains actin network (7).

Additionally, interactions of the cell with the surrounding matrix (ECM) have been shown experimentally (8,9) to affect the shape of cells (and even their differentiation (8,10)). In particular, the morphological features, such as the density and length of membrane protrusions, are affected by the rigidity of the ECM. The feature of the living cell primarily affected by the substrate rigidity is the adhesion of the cell to the substrate. It has also been observed that in the tips or along the length of protrusions, adhesion molecules (such as integrins) are concentrated (11–13). Since for these molecules to adhere they need to be connected to the actin cytoskeleton, their adhesion activity is also linked to the local level of actin polymerization (14). Both actin polymerization and the activity of molecular motors that enable adhesion are dependent on the metabolism of the cell.

One can therefore make the following model which proposes that: aggregation of some membrane proteins (MP), adhesion of the cell to the substrate, and actin polymerization near the membrane, must all be related in some way. The key feature that links the adhesion and actin polymerization to the membrane could be the spontaneous curvature of the membrane components. We implement these features by considering small protein complexes that have a convex spontaneous curvature, and also activate the polymerization of actin (15). Such protein complexes may include Formins, WASP, Arp2/3, and a host of proteins. Recently a number of membrane proteins that contain domains with specific spontaneous curvature, and are associated with actin filaments and polymerization, have been identified (15–17). These proteins are exactly the kind which we proposed to play a key role in our model (18). These membrane proteins are considered to be laterally mobile inside the membrane and permanently activated. Our model deals with their dynamics, which is treated as a two-dimensional gas in the plane of the membrane. We also consider that there may be attractive interactions between the MP, which also contribute to their aggregation (phase separation). The local density of these proteins is now coupled to the membrane shape deformation through the induced active forces and the spontaneous curvature. Another experimental example that links membrane convex curvature with actin-driven protrusions is Bettache et al. (19), where lipid composition is driving the spontaneous curvature.

Submitted May 22, 2007, and accepted for publication July 18, 2007.

Address reprint requests to Alex Veksler, Tel.: 972-8-934-6031; E-mail: alexander.veksler@weizmann.ac.il.

Editor: Alexander Mogilner.

0006-3495/07/12/3798/13 $2.00

doi: 10.1529/biophysj.107.113282

The proposed continuum model is based on the Helfrich Hamiltonian (20) for the membrane elastic energy, combined with the free energy of a gas of mobile membrane proteins, with the protrusive actin force added to the equations of motion. Our goal is to build a framework applicable for investigation of the various kinds of dynamic phase transitions and the formation of membrane protrusions in the living cells. In this model we consider dynamic-instability transitions in the coupled membrane-cortical cytoskeleton system. The cortical cytoskeleton is intimately coupled to the membrane and mainly composed of actin filaments. Physically, the appearance of instability means the phase separation of the MP, with the simultaneous formation of protrusions, and we therefore plot these transitions in the form of phase separation diagrams.

We do not consider all the intricate internal organization of the cell, such as its nucleus, microtubules, and intracellular organelles. Furthermore, we calculate here the instability of the membrane-cytoskeleton system within linear stability analysis, which is therefore limited to the initiation stage of any structural phase transitions. Such shape transitions may be followed by large-scale internal reorganization of the cell, over long timescales. These rearrangements are not treated within our phase transition model.

Membrane and vesicular deformation caused by proteins having intrinsic curvature was extensively studied during the last years (see, for example, (21–39)). However, it has been shown (24) that the bending energy coefficient must be very large, for the spontaneous curvature alone to be able to bring about phase separation and cause the appearance of membrane protrusions. Nevertheless, close to the critical temperature the curvature does enhance the phase separation, as was calculated (21) and observed (40). All these works investigated systems that are in thermodynamic equilibrium, where there are no active forces that arise from cellular metabolism (i.e., passive systems).

The effect of cell adhesion on the membrane shape was also studied, both experimentally and theoretically (12,13,31,32,41–45), and so was the effect of coupling the protrusive force of actin polymerization and spontaneous curvature (18,46–48). The main innovation of our work is the coupling of all these factors in one unified model. We have shown that, indeed, the protein phase separation and the formation of membrane protrusions may be driven by the cell adhesion and actin polymerization, rather than by the spontaneous curvature and aggregation alone. The results of our model introduce a new concept: dynamic-instability transitions in the coupled membrane-cortical cytoskeleton system can trigger shape changes in the cell, and maybe even influence the differentiation paths.

Let us stress here that our work deals with linear stability analysis of the system. We therefore consider adhesion and actin-driven protrusions in their initial stages of formation. The later stages, when mature focal adhesions and associated stress fibers form, are outside the scope of our work. The response of these structures to stress through their mechanosensitivity is also not treated here (49). We also consider that the elastic properties of the external substrate affect the adhesion strength, while other effects such as its elasticity and deformation (50), are neglected here. We nevertheless propose that the initial type of instability that initiates the formation of these later structures therefore determines the local or global cell shape. Our approach of linear stability analysis is somewhat similar to previous studies of shape instabilities in other fields of physics (51,52).

The model is developed in the next section and its linear stability analysis is further developed in the Appendix. In The Results: Stability Phase Diagrams, the various instability regimes are described in detail. Possible interpretation of the results, with comparison to experimental data, is given in Discussion and Conclusions.

THE MODEL

Model description

Our model is shown schematically in Fig. 1 *a*. We assume here that the membrane is approximately flat, which may apply to many cases, such as the leading edge of a cell that is spread on a substrate, a cell in suspension (spherical in shape), and the top and ventral sides of a spread cell. In all these cases, the scale of the cell curvature may be negligible as compared to that of the protrusions that we will describe. We assume that the cell is free to deform, so that curvature can play a role, as we show below.

In this flat membrane we assume a finite overall concentration of mobile clusters ϕ that include a variety of proteins,

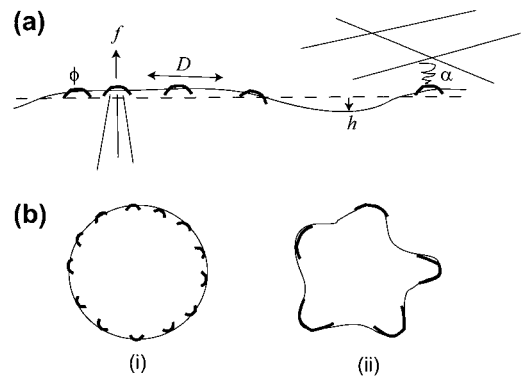

FIGURE 1 (*a*) A schematic picture of our model: an overall flat membrane (*solid line*) that is free to deform locally (h) and contains a population of membranal clusters (ϕ) that have a convex spontaneous curvature and are free to diffuse in the plane of the membrane with diffusion coefficient D. These membranal clusters (MPs) contain proteins that promote actin polymerization and protrusive force f, and adhesion to the surrounding ECM (inducing effective negative surface tension α). (*b*) The cell membrane-cortical cytoskeleton can be in the mixed state (*i*), which is featureless and uniform, or can become unstable (*ii*); phase-separated, with large aggregation of the MPs and protrusions/adhesions structures.

which are able to activate actin polymerization (protrusive force f in Fig. 1 *a*), and adhesion to the surrounding matrix (negative surface tension coefficient α). These clusters are free to diffuse in the plane of the membrane with effective diffusion coefficient D, which may be much smaller then for small membrane proteins, since there is the additional friction with the cytoskeleton. The effect of adhesion on the diffusion coefficient would lead to higher order (nonlinear) terms.

In our simple model we do not deal with the fast molecular timescales that build the cluster. We assume that the components of the cluster have some affinity, and that the resulting cluster therefore has both properties: actin polymerization and adhesion (in addition to having a spontaneous curvature) (4). The cluster that we describe may link adhesion with the promotion of actin polymerization by either a direct link or through some signaling cascade, while both lead to the same description. Note that there are many types of adhesions, and some, like those on the ventral side of the cell, may not be associated with a membrane protrusion, although all seem to be associated with actin polymerization (3).

In the specific system under consideration, the clusters (MPs) of membranal proteins are assumed to be sufficiently small to be described by a continuum model. This means that we are dealing with MPs that are much smaller than the lateral size of typical membrane protrusions, which are in the range of 100–1000 nm. Our MPs are, therefore, considered to have a lateral size of $a \sim 10$ nm. On the other hand, the radius of the spontaneous curvature of such clusters is assumed to be of the order of the lateral size of the protrusion, i.e., $R \sim 100$–1000 nm. This large value can be attributed to the fact that it is the radius of curvature of a membrane cluster (containing tens of proteins) and not of a single protein. Such aggregation curvatures have been recently reviewed in the literature (36,53,54).

In Fig. 1 *b*, we show schematically the two states of the membrane (or cell) that we obtain:

1. The mixed state. In this state, we have the clusters uniformly spread on the membrane, which therefore remains featureless and flat.
2. The phrase-separated state. This state occurs when the mixed state develops unstable modes, and the clusters are now aggregated and the membrane no longer flat.

Model equations

In this work we deal with an initially flat, infinite two-dimensional ($\vec{r} = (x, y)$) membrane. We assume that while the MP freely diffuse in the membrane, any hydrodynamical flow effects inside the highly viscous membrane fluid are neglected. The variables of the model are:

1. $h(\vec{r}, t)$, the local normal displacement of the membrane.
2. $\phi(\vec{r}, t)$, the local phase parameter of the MP, defined as $\phi \equiv n/n_S$, where $n(\vec{r}, t)$ is the local concentration and n_S is the saturation value (that is, $n_S \equiv a^{-2}$).

In this work we assume that the rigid actin cytoskeleton fully determines the membrane shape, and any small-scale thermal fluctuations in the membrane shape can therefore be neglected. We further assume that this cytoskeleton network suppresses long-range hydrodynamic flows on scales larger than the typical mesh-size $d \simeq 10$–100 nm, hence making all nonlocal effects negligible.

We write down the Helfrich's Hamiltonian (20) for the elastic energy of the membrane, including the direct effects of the MP concentration: spontaneous curvature and adhesion. The local spontaneous curvature is assumed to depend linearly on the MP concentration (second term in Eq. 1). The adhesion of MP to the ECM lowers the effective energy per unit membrane area, and therefore changes the surface tension term (first term in Eq. 1), in proportion to the concentration. To this elastic energy we add the terms that describe the gas of MP: its entropy (third term) and aggregation interaction (fourth term). The final free energy expression reads (21,55)

$$F = \int_S \left(\frac{1}{2}(\sigma - \alpha\phi)(\nabla h)^2 + \frac{\kappa}{2}\left(\nabla^2 h + \frac{\phi}{R}\right)^2 + \frac{T}{a^2}(\phi \ln \phi + (1-\phi)\ln(1-\phi)) + \frac{J}{2a^2}\phi(1-\phi) + \frac{J}{4}(\nabla\phi)^2 \right) d^2 r, \quad (1)$$

where S is the membrane area. Below we replace the full expression for the entropy by its expansion to fourth order in ϕ (Ginzburg-Landau approximation): $2((\phi - 1/2)^2 + 2/3(\phi - 1/2)^4)$. For simplicity, we assume in this work that the bending rigidity is only weakly dependent on the membrane composition.

The equations of motion for the membrane height displacement and for the protein phase are derived by variation of the free energy expression (Eq. 1) (56,57)

$$\frac{\partial h(\vec{r}, t)}{\partial t} = \int_S \left(-\frac{\delta F}{\delta h(\vec{r}', t)} + f(\phi(\vec{r}', t) - \phi_0) \right) \mathcal{O}(|\vec{r} - \vec{r}'|) d^2 r', \quad (2)$$

where the term $f(\phi(\vec{r}', t) - \phi_0)$ describes the protrusive force of actin polymerization acting on the membrane, while a uniform state ($h \equiv 0, \phi \equiv \phi_0$) remains stationary. In our model, f, σ, and α are assumed to be always positive.

For free membranes, $\mathcal{O}(|\vec{r} - \vec{r}'|) = (8\pi\eta|\vec{r} - \vec{r}'|)^{-1}$ is the diagonal portion of the Oseen tensor (58), and η is the effective viscosity coefficient of the ECM. Assuming confined hydrodynamic flows due to the cytoskeleton, of typical mesh-size d, we can simplify Eq. 2, by approximating the Oseen tensor by

$$\mathcal{O}(|\vec{r}-\vec{r}'|)=\begin{cases}(8\pi d\eta)^{-1}, & |\vec{r}-\vec{r}'|\le d\\ 0, & |\vec{r}-\vec{r}'|\ge d\end{cases}. \tag{3}$$

Consequently the integral is limited to the domain $|\vec{r}-\vec{r}'|\le d$, and the integrand is expanded around $\vec{r}'=\vec{r}$. To first order in d we get

$$\frac{\partial h(\vec{r},t)}{\partial t}=\frac{d}{8\eta}\left(-\frac{\delta F}{\delta h(\vec{r},t)}+f(\phi(\vec{r},t)-\phi_0)\right). \tag{4}$$

The dynamical equation for ϕ is also based on the variational derivative of the free energy, with the additional requirement of conservation of the total number of MPs. For simplicity we took $d\simeq a$ in the remainder of this article.

We therefore derive a diffusion equation for the density (56,57)

$$\frac{\partial\phi(\vec{r},t)}{\partial t}=\frac{Da^2}{T}\nabla\left(\phi(\vec{r},t)\nabla\frac{\delta F}{\delta\phi(\vec{r},t)}\right), \tag{5}$$

where D is the diffusion coefficient.

Note that the adhesion may also affect the effective viscosity of the membrane-substrate interface, namely making it dependent on $\phi(\vec{r},t)$ and α: $\eta\to\eta_0+g(\phi(\vec{r},t),\alpha)$, where g is some unknown increasing function of its variables. For simplicity, this effect is neglected here.

For clarity we prefer to work with nondimensional parameters, as follows: The two length scales in our problem are a and R, where their ratio, ε, is defined to be the small parameter of the system. We take R to be the unit length of the model, and set $a=\varepsilon R$. The room temperature, T_0, is defined to be the unit energy. The bending energy, κ, is taken to be $\kappa=\kappa' T_0$, and the temperature is $T=T' T_0$. We take a unit time to be the typical time of protein diffusion, $\tau_D\equiv R^2/D$. This value turns out to be very close to the typical time of the membrane height dynamics, $\tau_\eta\equiv\eta R^3/T_0$. Consequently, both dynamic coefficients can be nondimensionalized as $D=D'\,R^2/\tau$ ($D'=1$) and $\eta=\eta'\,T_0\,\tau/R^3$ ($\eta'=1.25$). The dimensions of σ and α are of energy density (J/m^2), hence they can be nondimensionalized by $\sigma=\sigma' T_0/R^2$ and $\alpha=\alpha' T_0/R^2$, while f has the dimension of pressure, and can be rewritten by $f=f' T_0/R^3$. The protein concentration parameter, ϕ, is nondimensional by definition, and it is convenient to shift it to the entropy and aggregation extremum, $\phi_0-1/2=\phi_0'$. We therefore work within small deviations from the equilibriam composition of $\phi_0=1/2$. The h variable becomes: $h=h'R$, and the space and time derivatives change to $\nabla\to\nabla/R$, $(\partial/\partial\mathrm{t})\to(\partial/\partial\mathrm{t})/\tau$.

The dynamical equations (Eqs. 4 and 5) can now be written in their final form, while omitting the primes for the rescaled parameters

$$\frac{\partial h}{\partial t}=\frac{\epsilon}{8\eta}\left(-\sigma\nabla^2 h-\alpha\nabla\left(\left(\phi+\frac{1}{2}\right)\nabla h\right)-\kappa\nabla^2(\phi+\nabla^2 h)+f(\phi-\phi_0)\right), \tag{6}$$

$$\frac{\partial\phi}{\partial t}=D\nabla\left(\left(\phi+\frac{1}{2}\right)\nabla\left((4T-J+\epsilon^2\kappa)\phi+\frac{16T}{3}\phi^3+\epsilon^2\left(\frac{\kappa}{2}-\frac{\alpha}{2}(\nabla h)^2+\kappa\nabla^2 h-\frac{J}{2}\nabla^2\phi\right)\right)\right). \tag{7}$$

We begin from a uniform initial state and look for conditions of instability. In our model, such instability means the onset of protein phase separation and the initiation of protrusions formation. The standard linear stability analysis is performed (37,38) where, for simplicity, the system is assumed to be nonuniform along one axis only. The variables h and ϕ are expanded around their initial homogeneous values, to first order: $h(x,t)=h_0+\delta h(x,t)$, $\phi(x,t)=\phi_0+\delta\phi(x,t)$, and substituted into the dynamical equations (Eqs. 6 and 7). Performing a space Fourier-transform, we get the linearized equations

$$\frac{\partial}{\partial t}\begin{pmatrix}\delta h(q,t)\\ \delta\phi(q,t)\end{pmatrix}=L\begin{pmatrix}\delta h(q,t)\\ \delta\phi(q,t)\end{pmatrix}L\equiv\begin{pmatrix}-\frac{\epsilon}{8\eta T_0}(\Sigma q^2+\kappa q^4) & \frac{\epsilon}{8\eta T_0}(f+\kappa q^2)\\ \frac{D}{T_0}\left(\phi_0+\frac{1}{2}\right)\epsilon^2\kappa q^4 & -\frac{D}{T_0}\left(\phi_0+\frac{1}{2}\right)\left((\mu+\epsilon^2\kappa)q^2+\frac{J}{2}\epsilon^2 q^4\right)\end{pmatrix}, \tag{8}$$

where two new parameters are defined

$$\Sigma\equiv\sigma-\alpha(\phi_0+1/2),\qquad \mu\equiv 4T(1+4\phi_0^2)-J. \tag{9}$$

The parameter Σ shows the competition between the positive surface tension σ and the average adhesion of the membrane, while μ shows the competition between the (temperature-induced) entropy and the aggregation interactions of the MP.

An unstable mode has positive growth rate $\omega_{1,2}(q)>0$. The conditions for instability occur in either one of the following cases:

1. Wave instability: $Tr\,(L)^2-4\,Det\,(L)=0$ and $Tr\,(L)>0$.
2. Turing instability: $Det\,(L)=0$ and $Tr\,(L)<0$.

In our model the wave instability occurs only for $f<0$, which we do not consider in this work (see, for example, (48)), so that the only possible kind of instability in our model is the Turing instability. The calculation details of the

conditions that give rise to this instability are given in the Appendix.

THE RESULTS: STABILITY PHASE DIAGRAMS

In this section we discuss the results of our model, in the form of stability phase diagrams (Figs. 2, 4, and 5); namely we plot the regions in the physical parameter space where the uniform system is stable, and where it is unstable. The regions where the uniform system is stable are called the mixed phase, since they correspond to a flat membrane and a uniform density ϕ_0 of the membrane complexes MP (Fig. 1 *b*). The unstable regions exhibit two types of instabilities: type-I and -II (Fig. 2), and there the uniform system breaks up (fragments) into aggregating complexes of MP, and growing membrane protrusions (Fig. 1 *b*). Since we are limited here to a linear stability analysis, we cannot predict the final new steady state (if one exists) of the system, as is usually the case for thermodynamic phase transitions. In the limit of the passive system (vanishing f and α), the thermodynamic phase transition occurs at the temperature where we find the first instability occurring (Fig. 3). Since we do not calculate the usual phase transition lines, there is no sense here to discuss the order of the transition, i.e., first or higher order. For the detailed analysis of the linear stability, we refer the reader to the Appendix.

The thermodynamic phase transition occurs at T_0 for a passive system ($f = \alpha = 0$) and flat membrane with zero surface tension, and turns out to be second-order. For finite surface tension the instability transition is shifted to a lower temperature, such that $T_{20} < T_0$ (Fig. 3). For consistency, we indeed find that this is the instability temperature we derive from our linear analysis (Eqs. 11 and 13) in this limit (for $\sigma = 0$). Note that as soon as the surface tension is finite, and inhibits the formation of membrane protrusions, the instability temperature is suppressed (Fig. 3 *b* and Fig. 6).

In the stability phase diagrams below we find two instability regions, where $\omega(q) > 0$ (Eq. 10). The physical meaning of both the instabilities is the same: the small protein complexes that initially were distributed homogeneously, start to aggregate, and protrusions start to appear on the initially flat membrane. However, the instability patterns are different, as shown in Fig. 2: type I is an instability band that starts at $q = 0$ and lasts until q_p (Fig. 2 *a*), with the most unstable mode at $q_p > q^* > 0$ (Eq. 11). At later times we expect that the system, which shows the type-I instability, to evolve toward global phase separation, where the size of the phase-separated domains increase to infinity ($q \to 0$), due to line tension (59). In a finite system, this will result in one phase-separated domain of proteins (H. Levine, private communication, 2007), while in a living cell the smallest mode is polar. This polarized structure of the real cell corresponds to two phase-separated domains on opposite sides, which allows that tensile forces are produced by molecular motors (myosin) to maintain the adhesion. The effects of these motors is not included in our model. Since in our model the domains also correspond to membrane protrusions and adhesion, they may remain separated and will not coalesce into one domain.

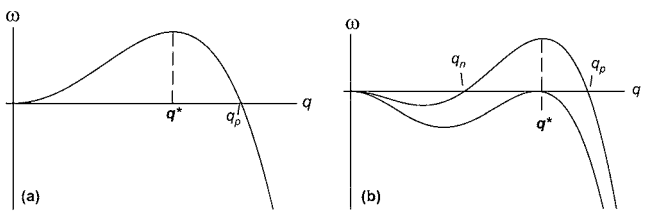

FIGURE 2 Instability patterns of the system. (*a*) Type-I instability: the instability band starts at $q = 0$, until q_p, and has a maximum at q^*. This instability leads to global phase-separation. (*b*) Type-II instability: the instability band first appears at q_c^*, and then grows into an unstable band. This instability gives rise to patterns with typical length scale.

On the other hand, in the type-II instability the wavevector in which we first get $\omega(q) > 0$ is at a nonzero value, denoted by Eq. 11, $q_c^* = \sqrt{-(2\kappa\mu + \epsilon^2 J\Sigma)/(2\epsilon^2 J\kappa)}$ (Fig. 2 *b*). The band of instability for type-II occurs for $q_n \le q \le q_p$ (Fig. 2 *b*). In these systems we therefore expect that the unstable domains remain with typical size $\sim 1/q^*$. Note that second-order phase transitions correspond to our type-I transition where $q^* = 0$ on the mixed-phase-separated transition line. There are examples of first-order phase transitions where a finite q^* appears at the transition line, similar to our type-II (51).

In all the diagrams below we use the following parameters: $\varepsilon = 0.05$, $\phi_0 = 1/2$, $J = 4$, and $\kappa = 10$. In Fig. 3 *a*, we plot the stability phase diagram in the actin activity (f) and reduced temperature (T/T_0) plane, for a fixed value of the adhesion strength (α), which is in the range $\alpha_0 > \alpha > \alpha_{cr}$. We find in this diagram the two kinds of instabilities we defined above: type-I occurs above the solid red line, while type-II instability occurs in the shaded region between the red and green lines. One finds for a sufficiently low temperature, $T < T_{10}$, a type-I instability that occurs even without the actin force ($f = 0$) or adhesion ($\alpha = 0$). This phenomenon means that in this region, the aggregation is the dominant term, and is sufficient to bring about an instability, which corresponds to phase separation at thermodynamic equilibrium, as was found previously (24). The transition temperature T_c of the passive system ($f = 0$, $\alpha = 0$) is T_{10} for $0 < \alpha_{cr}$; otherwise, it is given by T_{20}. In the range of the type-II instability we have competing contributions of comparable size from the aggregation, entropy, and elastic energies. Above the transition temperature, in the mixed state, the entropy is dominant over the aggregation and elastic energies.

For $\alpha_{cr} < 0$ (low surface tension) we have always a type-II instability for the passive system, while when $\alpha_{cr} > 0$ (high surface tension), this transition disappears for $\alpha_{cr} > \alpha$ (*blue solid line* in Fig. 3 *b*). Note that α_{cr} depends on the value of the surface tension σ (Eq. 15). We find that the slope of the

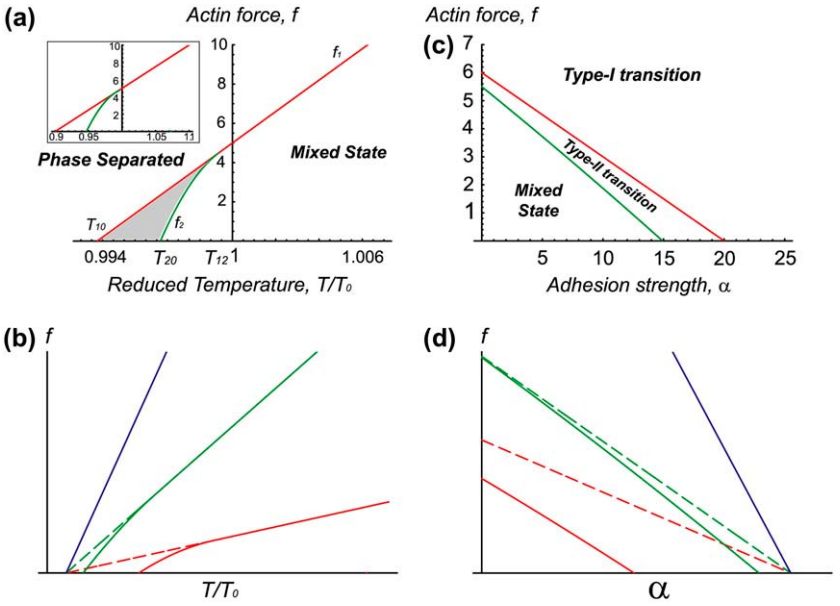

FIGURE 3 (*a* and *b*) Stability phase diagrams in the *f*-versus-*T* plane. The actin force leads to an increase in the critical temperature. The type-II instability is given by the shaded region. (*a*) We use $\sigma = 10$ and $\alpha = 10$. In all the graphs in this work we use $\varepsilon = 0.05$. In the inset of panel *a*, we plot the same diagram but now for $\varepsilon = 0.2$, and we find that the temperature range drastically increases. (*b*) The solid lines represent the phase-separation transition (*dashed lines* give the type II-type I transition), using $\sigma = 50$ and blue $\alpha = 0$, green $\alpha = 70$, and red $\alpha = 90$. The passive system is represented by the line $f \equiv 0$. (*c* and *d*) Stability phase diagrams in the *f*-versus-α plane. Here we find that increase in both *f* and α have a similar effect in driving the system into the unstable regime. (*c*) $T = 0.997T_0$ and $\sigma = 10$. (*d*) The solid lines represent the phase-separation transition (*dashed lines* give the type II-type I transition), using $\sigma = 10$ and blue $T = 1.005T_0$, green $T = 0.9985T_0$, and red $T = 0.997T_0$. For $\Sigma > \Sigma_{cr}$, only type-I instability is possible.

critical line decreases, and the passive transition temperature increases, with increasing values of the adhesion α. At α_0 the transition line becomes horizontal and the system is unstable at all temperatures. This means that when the adhesion is stronger than the surface tension, it is enough to bring about instability. The curved portion of the critical line (for small values of *f*) corresponds to the type-II instability transition (*green line* in Fig. 3 *a*). In Fig. 3 *c*, we plot the stability phase diagram in terms of *f* versus α, for a fixed temperature in the range $T_{10} < T < T_{12}$. In Fig. 3 *d*, we plot the *f*-α phase diagrams for different values of T/T_0. It can be easily seen that for $T/T_0 > T_{10}, T_{12}$, the type-II instability region disappears.

The most outstanding feature of this diagram is that the critical temperature increases linearly with the activity of the actin, above the critical temperature of the passive system. This linear relation follows from Eq. 13. Note that there is a large difference in the width of the unstable band above and below T_c; below this temperature, the band width increases linearly with decreasing temperature (Fig. 4, *b* and *d*); $q_p^2 \rightarrow -2(4T(1+4\phi_0^2) - J)/(\epsilon^2 J)$ (for $T/T_0 \ll 1$). In this limit, both *f* and α do not affect the asymptotic behavior of q_p. Above this temperature, the width is typically much smaller; for $\alpha > \alpha_0$, it approaches a constant $q_p^2 \rightarrow (\alpha(\phi_0 + 1/2) - \sigma)/\kappa$ for $T/T_0 \gg 1$ (*blue lines* in Fig. 4, *a* and *b*). Note that for $\alpha < \alpha_0$ there is always a finite critical temperature for all *f* (Fig. 4 *c*).

In the inset of Fig. 3 *a*, we show that a small increase in the ratio of the protein complex size *a* to its curvature radius *R*, i.e., in ε, results in a drastic increase in the temperature range of the transition. The critical temperatures increase above T_0 and decrease below T_0, as can be seen from Eq. 13 (note that $\mu = 0$ at T_0). Since the actin force promotes phase separation through the induction of curvature, increasing the curvature bending energy ($\propto \varepsilon^2\kappa$) increases the induced shift in the transition temperature. Note that the effect of actin force *f* shifts the critical temperatures by 1–10% (depending on ε), which translates to a shift of 1–10°C. For the larger ε, the shift in the transition temperature becomes measurable.

The next phase diagram that we plot is in terms of α versus temperature (Fig. 5). We see again that above α_0, the system is phase-separated for all temperatures; while below α_0, three is a critical temperature above which the system is mixed. In Fig. 5 *b*, we find that as the actin force is increased the critical temperature increases too, and the region of type-II instability is reduced, until it vanishes for large enough *f*. This is similar to the behavior seen in Fig. 3 *d*.

In Fig. 6, we plot the phase diagram in terms of the surface tension σ versus temperature. In Fig. 6 *a*, we keep the adhesion zero, while plotting the diagrams for different values of the actin force *f*. When *f* is negligible (*red lines*), we have a type-I instability below T_{10} independent of the surface tension, while the type-II instability vanishes (approaches T_{10}) when $\alpha_{cr} = 0$, i.e., at a critical surface tension $\sigma_{cr} = 2\kappa^2/J$ (Eq. 15). As the actin force increases, we find that the phase-separated region increases into higher values of σ, and the type-II region eventually vanishes altogether.

In Fig. 6 *b*, we plot the effects of adhesion, for negligible actin force. When increasing the adhesion strength, we find again that the unstable region exists for larger values of σ. Note that for $\sigma < \alpha\phi_0$ (i.e., for $\alpha > \alpha_0$) we have instability at all temperatures.

DISCUSSION AND CONCLUSIONS

To conclude, our work presented here is the first to calculate in a quantitative manner the spontaneous phase separation of membranal components which is driven by the forces of actin polymerization and adhesion. This phase separation is

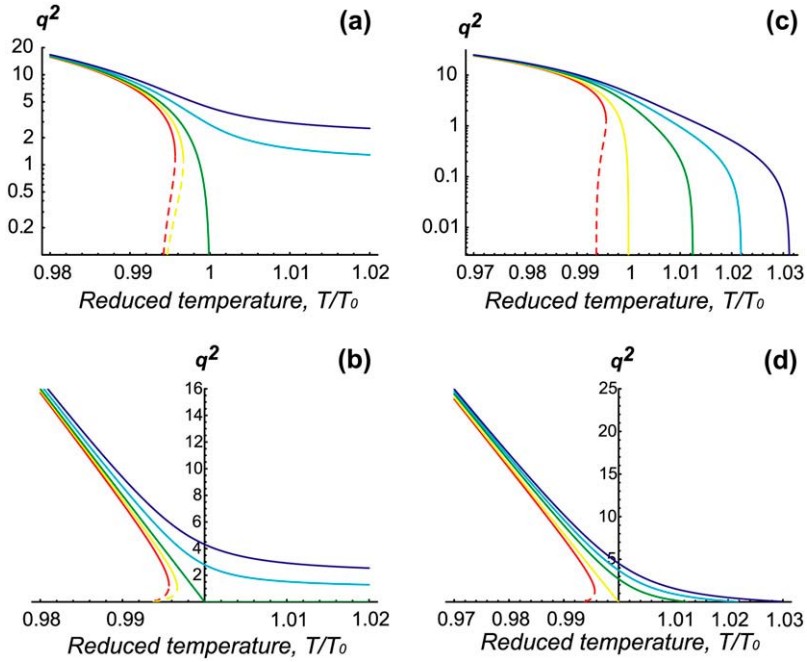

FIGURE 4 Graphs of q_p^2 versus T, for $\sigma = 10$ and various values of f and α. (*a*) $f = 0$, α grows counterclockwise ($\alpha = 0$, 10, 20, 40, 60); the scale is Log (q_p^2) versus linear (T). (*b*) Same graph as panel *a*, but on linear-linear scale. The solid line give q_p while the dashed lines give q_n. Both are in units of $1/R$, where $R = 100$ nm. (*c*) $\alpha = 0$, f grows counterclockwise ($f = 0$, 10, 30, 45, 60); the scale is Log (q_p^2) versus linear (T); the cutoff temperature is $T_{cut} = (J(\sigma - \alpha(\phi_0 + 1/2)) + \varepsilon^2\kappa(f + \alpha\,(\phi_0 + 1/2) - \sigma))/(4(\sigma - \alpha(\phi_0 + 1/2))(1 + 4\,\phi_0^2))$. (*d*) Same graph as panel *c*, but on linear-linear scale; again, q_p^2 has the same linear asymptotic dependence on T for $T \ll T_0$.

tightly linked with the formation of membrane curvature, and we therefore propose that it is the driving force for many cellular shape transformations. One limitation of our model is that in its present form it does not describe the behavior of cells inside a three-dimensional matrix (61,62).

We now give several experimental observations that seem to exhibit the phase separation we calculated above.

We begin with a more simple artificial system that was recently observed (7). In this work, synthetic vesicles, containing a number of reconstituted proteins that are known to activate actin polymerization in cell, were observed as a function of temperature. It was found that the phase-separation temperature increased by ~8°C when actin monomers were added into the buffer and formed a network of filaments on the outer surface of the membrane. This behavior is in qualitative agreement with our calculation of Fig. 3 *a*, where we predict that the actin force enhances the critical temperature. Note that, alternatively, the effect of the actin network may be to increase the effective attractive interaction J between the membrane proteins, and therefore increase the critical temperature independently of the actin polymerization force f, i.e., independent of any metabolism. Such synthetic in vitro systems offer a good platform to test our model, since they allow good control over the different model parameters.

We next give a few examples from living cells. Note first that in a living cell there may be a number of types of membranal proteins and complexes that have different values of curvature (R), density (ϕ_0), and activity (f and α) (15,17). Each such type of MP therefore has different phase transition conditions, and in a real cell membrane there can therefore be a number of phase-separation transitions. Second, our model assumes a uniform system, which therefore corresponds to cases where the active part of the cell membrane is uniform; for example, the lamellipodia of motile cells has a rather uniform leading edge, the growth cone of axons (63), and possibly the entire cell periphery in adhering (nonmotile) cells. In all these cases, structural phase transitions that lead to the formation of protrusions, membrane phase separation, and adhesion loci, may be examples where our model applies.

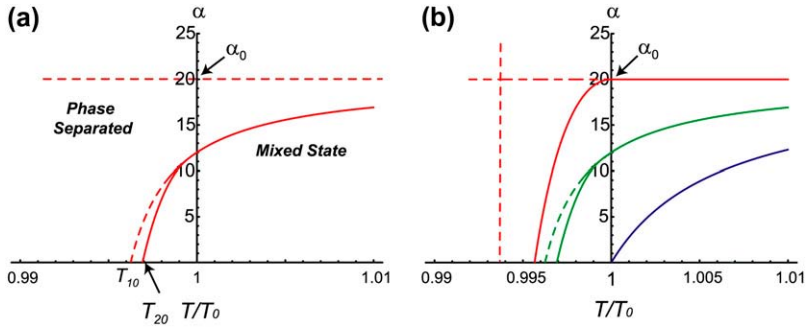

FIGURE 5 Stability phase diagram in the adhesion(α)-temperature plane. We find that the adhesion can drive the instability, increasing the transition temperature. (*a*) General features of the phase transition line (*solid line*), for $f = 4$. The shaded region shows the type-II instability (bounded by *solid* and *dashed lines*). The passive system is represented by the x axis where $\alpha = 0$. At α_0 (*horizontal dashed line*) the transition temperature diverges. (*b*) Transitions lines (*solid line*) for various values of the actin force f: from top to bottom, $f = 0$, 4, 10.

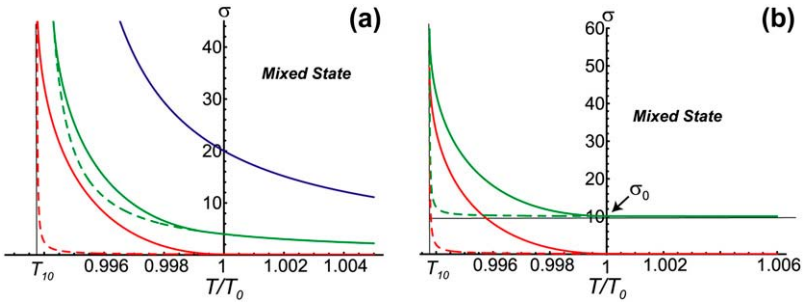

FIGURE 6 Stability phase diagram in the surface-tension(σ)-temperature plane. We find that the increase in the surface tension decreases the instability temperature below the thermodynamic phase transition temperature. Increasing f or α increases again the instability temperature. (*a*) Phase-separation lines (*solid lines*) for various values of f (and zero adhesion $\alpha = 0$); from top to bottom, $f = 20, 4, 0.1$. The dashed lines give the transition between type-II and type-I instability. (*b*) Phase-separation lines (*solid lines*) for various values of α (and negligible actin force $f = 0.1$); from top to bottom, $\alpha = 20, 0$. The dashed lines give the region of type-II instability. The horizontal black line indicates the value $\sigma = \alpha\phi_0$, below which the system is unstable at all temperatures. The vertical black line gives the lower critical temperature T_{10}, below which the system is unstable (type-I) for all surface tensions.

Furthermore, a cell may change its overall shape and motility due to small changes in the internal expression of the components that drive the shape transitions, i.e., in our model the actin and adhesion mechanisms. This may explain the observation that identical cells from a single culture display a number of morphologies, and even individual cells change between these different shapes (64,65). It is further shown that these different morphologies are closely related to marked changes in the cell's actin and adhesion organization.

Another example of striking shape transformations is given in Baas et al. (66), where expression of a protein that is connected with the activation of the actin cytoskeleton changes the cell shape from an adhering starlike shape to a compact form that has the entire cortical actin phase separated into a single domain of tightly packed microvilli projections. Within our model this transfers the cell from a type-II instability due to adhesion (α) to a type-I instability due to actin force (f) (Fig. 7 *a*).

1. In Runge et al. (67), it was found that membrane receptors (CD9) exclusively aggregate at high concentrations on the surface of microvilli, which are membrane protrusions that are driven by actin polymerization. The activity of these receptors inside the microvilli enhance their length, and therefore within our model they may be considered as part of the complex of MP that enhance the actin protrusive force. Whether the complex containing these receptors also has the convex spontaneous curvature, remains to be experimentally tested.
2. In the growth-cone of axons (63) it was observed that, in the absence of myosin, the filopodia are highly static and appear to be regularly spaced. If indeed our model is correct, then this typical spacing between the filopodia is given by the $1/q^*$ that we calculate. The static nature of these filopodia, i.e., their lack of lateral motion along the front edge of the growth cone, arises naturally in our model, where only Turing instability arises. When myosin is active there is a possibility for wave instability (48).
3. Another example where a combination of spontaneous curvature and actin polymerization may be driving phase separation, is in the formation of the immune synapse (2,68,69). The spontaneous curvature of the TCR microcomplexes is due to their closer adhesion to the neighboring cell, as compared to the surrounding membrane. They are also observed to be regions of high actin polymerization activity, and indeed they aggregate to form the large immune synapse. We therefore propose that the aggregation of these complexes is triggered by an increase in f, as shown in Fig. 3 *a*.
4. In cell-cell junctions the cadherin molecules need to form a large aggregate to stabilize the adhesion (70–72). It is further shown that when the link between the cadherins and the actin cytoskeleton is broken, this aggregation cannot take place. We propose that this is another example where adhesion and actin-driven protrusion combine to give phase separation and aggregation in the membrane.
5. In motile cells the leading edge of the lamellipodia has a relatively large convex curvature in its cross section, and strong actin polymerization activity. It was found that in this region there is a membranal complex that prevents lipid diffusion through the leading edge (73). This densely packed complex disintegrates when the actin polymerization is inhibited, while keeping the high curvature artificially. This may correspond to our results of Fig. 3 *a*, where the actin force enables the system to phase-separate even when the passive system is mixed. The curvature alone may not be sufficient to cause phase separation, as we discussed above.
6. Experiments on the effects of the external substrate on the shape of cells have been carried out in recent years (8,9). In one experiment (8) it was found that astrocytes change their shape from approximately round on soft substrate to jagged (triangular) on a hard substrate. Within our model this shape transition corresponds to the phase separation we calculated; the round cells correspond to the mixed phase, while the polygonal shapes correspond to the phase-separated state, since phase-separated domains correspond to membrane protrusions. Since these cells adhere more strongly on harder surfaces (74,75), this phase transition may be driven by an

increase of α, as is shown in Fig. 2 *c* and Figs. 4 and 7. Similar transitions were observed in fibroblast cells (12,13), where the higher the adhesion (substrate rigidity), the more numerous the cell protrusions (starlike shapes). This corresponds to the increase in q_p, q^*, the more unstable the system is (Fig. 4, *a* and *b*, and Fig. 7). A similar trend of increase in the density of protrusions with the adhesion strength was observed in Cukierman et al. (76).

On the other hand, the changes in shapes in response to the increase in stiffness and adhesion can be more complicated (10,77). It is observed that as the substrate stiffens, the cell's protrusions bundle and the star-shape is transformed into a polarized dipolar body. This transition is indicated by the shapes drawn in Fig. 7. We interpret these changes in the following way: the star-shape is typical for cells that are close to the mix-type-II transition, with protrusions at the wavelength corresponding to the dominant mode q^*. As the adhesion increases and they move to larger values of α, larger wavelength modes become unstable (q_n decreases; see Fig. 7 *c*) and mix with the dominant mode, producing aggregation of the protrusions. Finally, when $1/q_n$ becomes larger than the cell circumference, the lowest mode (a force dipole) dominates the large-scale ordering of the protrusions. This polarized structure of the real cell corresponds to two phase-separated domains on opposite sides, which allows tensile forces produced by molecular motors (myosin) to maintain the adhesion. The effects of these motors is not included in our model.

Adhesion to the substrate was shown to determine the overall fate of cells, to either proliferation or apoptosis (78). In particular it seems that when the cells are confined to compact shapes the adhesions are weak, and no large aggregations of adhesion and actin are observed. When cells are allowed to deform, their adhesion clusters are usually in highly curved membrane protrusions, where strong aggregation of adhesion molecules and actin is observed. It may well be that only when cell deformation is allowed does the phase separation of membrane components occur due to coupling of membrane shape and active forces as our model predicts. This phase separation and aggregation of proteins can trigger the signals (79) that determine the cell's fate.

7. It was further found that the substrate rigidity influences not only the cell shape but also its differentiation, in the case of stem cells (8,10). It will be interesting in the future to investigate the interplay between the stability phase transition that we calculated, which occurs in the cytoskeleton and membrane, and the resulting changes in the cell differentiation and genetic expression. Since the cell membrane may contain a number of types of MP, and therefore experience a number of phase transitions as a function of adhesion strength, each such transition may trigger another change in the differentiation path. Through these different transitions at the membrane-cortical cytoskeleton the cell may respond differently to different external substrates. An interesting conjecture may be that the round and featureless stem cells have no stable membranal domains and segregation, due to many competing forces. When the cell differentiates some genes are expressed more then others and consequently some protein-networks can become dominant and lead to membranal phase transitions, as we described. There may therefore be a positive feedback loop between the cytoskeleton-membrane transitions and the expression of genes, which leads to differentiation.

It is interesting to think of a mapping between the structural phase transitions in the cell membrane-cortical cytoskeleton and genetic phase transitions. Such a mapping relates the cell response to the external substrate to the differentiation path it chooses. Our model gives also a plausible mechanism by which cells form specific membranal domains that are well

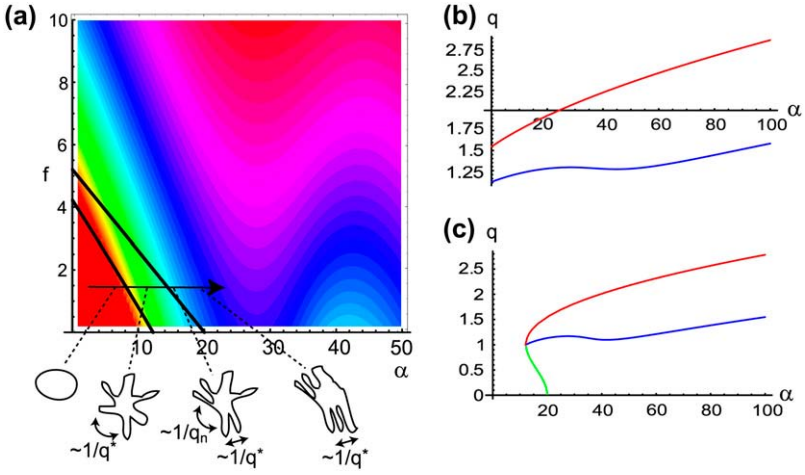

FIGURE 7 (*a*) Contours of the wavevector of the most unstable mode q^* in the (α, f) stability phase diagram ($T = 0.997T_0$). The heavy black dashed line shows the mixed-type-II phase transition and the heavy solid black line shows the type-II → type-I phase transition. In panels *b* and *c*, we plot the wavevectors of the unstable region (q^*, *blue line*; q_p, *red line*; and q_n, *green line*) for $f = 10$ and $f = 0$, respectively (the wavevectors are in units of $1/R$, where $R = 100$ nm). Below the contour plot, we show the expected shapes of cells along the trajectory indicated by the heavy arrow.

segregated and driven by both actin polymerization and adhesion. These domains serve to initiate a signaling cascade that influences the cell's behavior (for example, the T-cell (69)), gene expression (62), and malignancy (80,81). Interfering with the ability of the cell to form these domains, by disrupting the actin polymerization and adhesion, will allow us to modify the cell behavior and fate.

We now wish to suggest a number of testable predictions that may test the validity of our model:

- The most direct test of our model will be the detailed characterization of the clusters that are involved in promoting protrusions and adhesion, and finding if indeed these have the spontaneous curvature that we assumed in our model.
- In vitro experiments of the kind described in Liu and Fletcher (7) may be repeated using recently discovered proteins that are known to have convex curvature and associate with actin filaments (16). In such a system, the phase-separation transition with and without actin polymerization may be measured and test our prediction of Fig. 3.
- For the filopodia in the growth-cone of axons (63) (with myosin blocked), we predict that the spacing should decrease if the actin force f is increased, or if the adhesion is increased, or if the surface tension is decreased. This may be tested in future experiments.
- In the case of type-II instability, we predict that the wavelength of the protrusions will increase with increasing surface tension (Fig. 4). This may be tested on cells that exhibit filopodia and microvilli, to test that not only their amplitude, but their density, decreases with increasing induced surface tension.
- Similarly, increasing the adhesion strength (by chemical or biological means), should result in an increase in the density of adhesion-related structures, such as podosomes.
- We further expect that increasing the surface tension suppresses the formation of phase separation and protrusions (Fig. 6), which can be tested in both living cells and in vitro synthetic systems.

APPENDIX: LINEAR STABILITY ANALYSIS

In this Appendix, we give the details of the linear stability analysis of The Model, detailed above.

Equation 8 is an eigenvalue problem, with the solution

$$\omega_{1,2}(q)=\frac{1}{2}\left(Tr(L)\pm\sqrt{Tr(L)^2-4Det(L)}\right). \qquad (10)$$

To obtain the conditions for Turing instability, we need to calculate the roots of $Det\ (L)$ and $Tr\ (L)$. The solutions of $Det\ (L)=0$ are

$$q^2=0,\quad q^2_{\mathrm{p,n}}=s\sqrt{\frac{2}{J}(f_1-f_2)}\pm\sqrt{\frac{2}{J}(f-f_2)}, \qquad (11)$$

where we set $q^2_{\mathrm{n}}\le q^2_{\mathrm{p}}$. The f-values are given by

$$f_1\equiv\left(1+\frac{\mu}{\epsilon^2\kappa}\right)\Sigma$$
$$f_2\equiv f_1-\frac{(\mu_{12}-\mu)^2}{2\epsilon^4 J}, \qquad (12)$$

where $\mu_{12}\equiv-\varepsilon^2 J\Sigma/2\kappa$, and

$$s=\begin{cases}+1, & \mu<\mu_{12}\\ -1, & \mu>\mu_{12}\end{cases}. \qquad (13)$$

The roots of $Tr\ (L)$ are given by

$$q^2=0,\quad q^2_{\mathrm{tr}}=-\frac{8D\eta(\phi_0+1/2)(\mu+\epsilon^2\kappa)+\epsilon\Sigma}{4\epsilon^2 D\eta J(\phi_0+1/2)+\epsilon\kappa}. \qquad (14)$$

Omitting the unessential technical details, we derive here the conditions which must hold together, for q^2_{p} or q^2_{n} to correspond to an instability transition point: 1), it must be real and positive; and 2), it must be larger than q^2_{tr}. Note that at $q=0$, the growth rate is always zero. It should be noted that in the stability analysis, only real wavenumbers are meaningful. Hence, only real and positive q^2 can be accepted. In addition, it can be easily seen from Eq. 8 that for large q, $Det\ (L)>0$, and $Tr(L)<0$, and the system is always stable.

The physical parameters of the system may be divided into two sets:

1. The temperature T, average protein concentration ϕ_0, aggregation potential J, and surface tension σ are all intrinsic parameters of fluid membranes, both in synthetic (passive) systems and in living cells.
2. The adhesion strength α and actin force f are parameters that arise from metabolic activity and are therefore unique to the living system.

The control parameters of our model turn out to be μ, f, and Σ (Eq. 9). Two of them, μ and Σ, are a combination of physical parameters. For example, the relative increase of entropy with respect to the aggregation will change μ, but their simultaneous increase will not. In the phase diagrams that we plot below, the variation in μ is due only to variation in the temperature T, while keeping ϕ_0 and J constant. We further assume that only the entropy changes with the temperature, while all the other parameters are temperature-independent. This means that a change of T means a change of balance between the aggregation (J) and the entropy. Under these assumptions, the variation of the model parameters μ, Σ, and f corresponds to the variation of the physical parameters T, α, σ, and f. The phase diagrams will be given in terms of the physical parameters.

Moreover, for the sake of simplicity, we choose the aggregation coefficient J to yield $\mu=0$ for $T=T_0$, which is the temperature for which the entropy is equal to the aggregation. In most biologically relevant systems T_0 is of the order of room temperature (7). Note that the adhesion can be both stronger or weaker (on average) than the surface tension, resulting in either positive or negative Σ (Eq. 9). Strong adhesion and formation of protrusions drives an increase in the apparent membrane area, which results in an exponential increase of the surface tension coefficient σ in a closed system of finite overall membrane area (82). This feedback mechanism between the surface tension and the adhesion is a nonlocal effect, so it is not included in our model. We may conclude that this effect confines the range of possible values to $\alpha<\alpha_0$ (see below). Note that this effect limits the growth of all membranal protrusions, as observed for example in Bohil et al. (83).

For the presentation of the stability phase diagrams, the following parameters should be defined as

$$\alpha_0 = \sigma/\phi_0; \quad \alpha_{cr} = \frac{\sigma - 2\kappa^2/J}{\phi_0 + 1/2}; \quad T_{10} = \frac{J - \epsilon^2\kappa}{4(1+4\phi^2)}$$

$$T_{12} = -\frac{J(2\kappa - \epsilon^2\Sigma)}{8\kappa(1+4\phi^2)}; \quad T_{20} = \frac{J - \epsilon^2(\sqrt{2J(\sigma - \alpha(\phi_0 + 1/2))} - J(\sigma - \alpha(\phi_0 + 1/2))/2\kappa)}{4(1+4\phi_0^2)}, \tag{15}$$

where α_0 is the point where the cell-substrate adhesion is equal (on average) to the surface tension. The value α_{cr} will be clarified in the following: T_{10} and T_{20} are the vanishing points of f_1 and f_2, respectively. The value T_{12} is the touching point of f_1 with f_2.

We thank Sam Safran and Patricia Bassereau for useful discussions and David Andelman for useful comments.

We thank the European Union Comp NoE grant and the Alvin and Gertrude Levine Career Development Chair for their support. This research was supported by the Israel Science Foundation (grant No. 337-05).

REFERENCES

1 Revenu, C., R. Athman, S. Robine, and D. Louvard. 2004. The co-workers of actin filaments: from cell structures to signals. *Nat. Rev. Mol. Cell Biol.* 5:1–12.

2. Razzaq, T., P. Ozegbe, E. C. Jury, P. Sembi, N. M. Blackwell, and P. S. Kabouridis. 2004. Regulation of T-cell receptor signaling by membrane microdomains. *Immunology.* 113:413–426.
3. Brown, E. J. 2002. Integrin-associated proteins. *Curr. Opin. Cell Biol.* 14:603–607.
4. Schirenbeck, A., R. Arasada, T. Bretschneider, M. Schleicher, and J. Faix. 2005. Formins and VASPs may co-operate in the formation of filopodia. *Biochem. Soc. Trans.* 33:1256–1259.
5. Belyantseva, I. A., E. T. Boger, S. Naz, G. I. Frolenkov, J. R. Sellers, Z. M. Ahmed, A. J. Griffith, and T. B. Friedman. 2005. Myosin-XVa is required for tip localization of whirlin and differential elongation of hair-cell stereocilia. *Nat. Cell Biol.* 7:148–156.
6. Parthasarathy, R., C. H. Yu, and J. T. Groves. 2006. Curvature-modulated phase separation in lipid bilayer membranes. *Langmuir.* 22:5095–5099.
7. Liu, A. P., and D. A. Fletcher. 2006. Actin polymerization serves as a membrane domain switch in model lipid bilayers. *Biophys. J.* 91: 4064–4070.
8. Georges, P. C., W. J. Miller, D. F. Meaney, E. S. Sawyer, and P. A. Janmey. 2006. Matrices with compliance comparable to that of brain tissue select neuronal over glial growth in mixed cortical cultures. *Biophys. J.* 90:3012–3018.
9. Discher, D. E., P. Janmey, and Y. L. Wang. 2005. Tissue cells feel and respond to the stiffness of their substrate. *Science.* 310:1139–1143.
10. Engler, A. J., S. Sen, H. L. Sweeney, and D. E. Discher. 2006. Matrix elasticity directs stem cell lineage specification. *Cell.* 126: 677–689.
11. Martins, G. G., and J. Kolega. 2006. Endothelial cell protrusion and migration in three-dimensional collagen matrices. *Cell Motil. Cytoskeleton.* 63:101–115.
12. Jiang, G., A. H. Huang, Y. Cai, M. Tanase, and M. P. Sheetz. 2006. Rigidity sensing at the leading edge through $\alpha_v\beta_3$ integrins and *RPTPα*. *Biophys. J.* 90:1804–1809.
13. Giannone, G., and M. P. Sheetz. 2006. Substrate rigidity and force define form through tyrosine phosphatase and kinase pathways. *Trends Cell Biol.* 16:213–223.
14. Hall, A. 2005. ρ-GTPases and the control of cell behavior. *Biochem. Soc. Trans.* 33:891–895.
15. Takenawa, T., and S. Suetsugu. 2007. The WASP-WAVE protein network: connecting the membrane to the cytoskeleton. *Nat. Rev. Mol. Cell Biol.* 8:37–48.
16. Mattila, P. K., A. Pykalainen, J. Saarikangas, V. O. Paavilainen, H. Vihinen, E. Jokitalo, and P. Lappalainen. 2007. Missing-in-metastasis and IRSp53 deform PI(4,5)P2-rich membranes by an inverse BAR domain-like mechanism. *J. Cell Biol.* 176:953–964.
17. Itoh, T., and P. D. Camilli. 2006. BAR, F-BAR (EFC) and ENTH/ANTH domains in the regulation of membrane-cytosol interfaces and membrane curvature. *Biochim. Biophys. Acta.* 1761:897–912.
18. Gov, N. S., and A. Gopinathan. 2006. Dynamics of membranes driven by actin polymerization. *Biophys. J.* 90:454–469.
19. Bettache, N., L. Baisamy, S. Baghdiguian, B. Payrastre, P. Mangeat, and A. Bienvenue. 2003. Mechanical constraint imposed on plasma membrane through transverse phospholipid imbalance induces reversible actin polymerization via phosphoinositide 3-kinase activation. *J. Cell Sci.* 116:2277–2284.
20. Helfrich, W. 1974. Blocked lipid exchange in bilayers and its possible influence on the shape of vesicles. *Z. Naturforsch.* [*C*]. 29: 510–515.
21. Leibler, S., and D. Andelman. 1987. Ordered and curved mesostructures in membranes and amphiphilic films. *J. Phys.* 48:2013–2018.
22. Safran, S. A., P. Pincus, and D. Andelman. 1990. Theory of spontaneous vesicle formation in surfactant mixtures. *Science.* 248:354–356.
23. Safran, S. A., P. A. Pincus, D. Andelman, and F. C. MacKintosh. 1991. Stability and phase behavior of mixed surfactant vesicles. *Phys. Rev. A.* 43:1071–1078.
24. MacKintosh, F. C., and S. A. Safran. 1993. Phase separation and curvature of bilayer membranes. *Phys. Rev. E Stat. Phys. Plasmas Fluids Relat. Interdiscip. Topics.* 47:1180–1183.
25. Seifert, U., K. Berndl, and R. Lipowsky. 1991. Shape transformations of vesicles: phase diagram for spontaneous-curvature and bilayer-coupling models. *Phys. Rev. A.* 44:1182–1202.
26. Jülicher, F., and R. Lipowsky. 1993. Domain-induced budding of vesicles. *Phys. Rev. Lett.* 70:2964–2967.
27. Jülicher, F., and R. Lipowsky. 1996. Shape transformations of vesicles with intramembrane domains. *Phys. Rev. E Stat. Phys. Plasmas Fluids Relat. Interdiscip. Topics.* 53:2670–2683.
28. Kumar, P. B. S., G. Gompper, and R. Lipowsky. 2001. Budding dynamics of multicomponent membranes. *Phys. Rev. Lett.* 86:3911–3914.
29. Sackmann, E. 1995. Physical basis of self-organization and function of membranes: physics of vesicles. *In* Handbook of Biological Physics, Vol. 1. R. Lipowsky and E. Sackmann, editors. Elsevier Science, New York. 213–303.
30. Safran, S. A. 1999. Curvature elasticity of thin films. *Adv. Phys.* 48: 395–448.
31. Seifert, U. 1993. Curvature-induced lateral phase segregation in two-component vesicles. *Phys. Rev. Lett.* 70:1335–1338.
32. Seifert, U. 2004. Fluid Vesicles. Lecture Notes: ''Physics Meets Biology. From Soft Matter to Cell Biology''. 35th Spring School, Jülich, Germany.
33. Evans, A. R., M. S. Turner, and P. Sens. 2003. Interactions between proteins bound to biomembranes. *Phys. Rev. E Stat. Nonlin. Soft Matter Phys.* 67:041907.

34. Sens, P., and M. Turner. 2004. Theoretical model for the formation of caveolae and similar membrane invaginations. *Biophys. J.* 86:2049–2057.
35. Sens, P., and M. Turner. 2006. Budded membrane microdomains as tension regulators. *Phys. Rev. E Stat. Nonlin. Soft Matter Phys.* 73:031918.
36. Sens, P. 2004. Dynamics of nonequilibrium membrane bud formation. *Phys. Rev. Lett.* 93:108103.
37. Reigada, R., J. Buceta, and K. Lindenberg. 2005. Nonequilibrium patterns and shape fluctuations in reactive membranes. *Phys. Rev. E Stat. Nonlin. Soft Matter Phys.* 71:051906.
38. Reigada, R., J. Buceta, and K. Lindenberg. 2005. Generation of dynamic structures in nonequilibrium reactive bilayers. *Phys. Rev. E Stat. Nonlin. Soft Matter Phys.* 72:051921.
39. Božič, B., V. Kralj-Iglič, and S. Svetina. 2005. Coupling between vesicle shape and lateral distribution of mobile membrane inclusions. *Phys. Rev. E Stat. Nonlin. Soft Matter Phys.* 73:041915.
40. Roux, A., D. Cuvelier, P. Nassoy, J. Prost, P. Bassereau, and B. Goud. 2005. Role of curvature and phase transition in lipid sorting and fission of membrane tubules. *EMBO J.* 24:1537–1545.
41. Lipowsky, R. 1996. Adhesion of membranes via anchored stickers. *Phys. Rev. Lett.* 77:1652–1655.
42. Menes, R., and S. A. Safran. 1997. Nonlinear response of membranes to pinning sites. *Phys. Rev. E Stat. Phys. Plasmas Fluids Relat. Interdiscip. Topics.* 56:1891–1899.
43. Durand, I., P. Jonson, C. Misbah, A. Valance, and K. Kassner. 1997. Adhesion-induced vesicle propulsion. *Phys. Rev. E Stat. Phys. Plasmas Fluids Relat. Interdiscip. Topics.* 56:R3776–R3779.
44. Bruinsma, R., A. Behrisch, and E. Sackmann. 2000. Adhesive switching of membranes: experiment and theory. *Phys. Rev. E Stat. Phys. Plasmas Fluids Relat. Interdiscip. Topics.* 61:4253–4267.
45. Rózycki, B., T. R. Weikl, and R. Lipowsky. 2006. Adhesion of membranes via switchable molecules. *Phys. Rev. E Stat. Nonlin. Soft Matter Phys.* 73:061908.
46. Atilgan, E., D. Wirtz, and S. X. Sun. 2005. Morphology of the lamellipodium and organization of actin filaments at the leading edge of crawling cells. *Biophys. J.* 89:3589–3602.
47. Gov, N. S. 2006. Dynamics and morphology of microvilli driven by actin polymerization. *Phys. Rev. Lett.* 97:018101.
48. Shlomovitz, R., and N. S. Gov. 2007. Membrane waves driven by actin and myosin. *Phys. Rev. Lett.* 98:168103.
49. Bershadsky, A., M. Kozlov, and B. Geiger. 2006. Adhesion-mediated mechanosensitivity: a time to experiment, and a time to theorize. *Curr. Opin. Cell Biol.* 18:472–481.
50. Safran, S. A., N. S. Gov, A. Nicolas, U. S. Schwarz, and T. Tlusty. 2005. Physics of cell elasticity, shape, and adhesion. *Physica A.* 352:171–201.
51. Seul, M., and D. Andelman. 1995. Domain shapes and patterns: the phenomenology of modulated phases. *Science.* 267:476–483.
52. Langer, S., R. Goldstein, and D. Jackson. 1992. Dynamics of labyrinthine pattern formation in magnetic fluids. *Phys. Rev. A.* 46:4894–4904.
53. Zimmerberg, J., and M. M. Kozlov. 2006. How proteins produce cellular membrane curvature. *Nat. Rev. Mol. Cell Biol.* 7:9–19.
54. Huang, K. C., R. Mukhopadhyay, and N. S. Wingreen. 2006. A curvature-mediated mechanism for localization of lipids to bacterial poles. *PLoS Comput. Biol.* 2:1357–1364.
55. Safran, S. A. 2003. Statistical Thermodynamics of Surfaces, Interfaces, and Membranes. Westview Press, Boulder, CO.
56. Ramaswamy, S., J. Toner, and J. Prost. 2000. Nonequilibrium fluctuations, traveling waves, and instabilities in active membranes. *Phys. Rev. Lett.* 84:3494–3497.
57. Ramaswamy, S., and M. Rao. 2001. The physics of active membranes. *C. R. Acad. Sci. Série IV.* 2:817–839.
58. Gov, N., A. G. Zilman, and S. Safran. 2004. Hydrodynamics of confined membranes. *Phys. Rev. E Stat. Nonlin. Soft Matter Phys.* 70:011104.
59. Tian, A., C. Johnson, W. Wang, and T. Baumgart. 2007. Line tension at fluid membrane domain boundaries measured by micropipette aspiration. *Phys. Rev. Lett.* 98:208102.
60. Reference deleted in proof.
61. Ahmed, I., A. S. Ponery, A. Nur-E-Kamal, J. Kamal, A. S. Meshel, M. P. Sheetz, M. Schindler, and S. Meiners. 2007. Morphology, cytoskeletal organization, and myosin dynamics of mouse embryonic fibroblasts cultured on nanofibrillar surfaces. *Mol. Cell. Biochem.* 301:241–249.
62. Li, G. N., L. L. Livi, C. M. Gourd, E. S. Deweerd, and D. Hoffman-Kim. 2007. Genomic and morphological changes of neuroblastoma cells in response to three-dimensional matrices. *Tissue Eng.* 13:1035–1047.
63. Medeiros, N. A., D. T. Burnette, and P. Forscher. 2006. Myosin II functions in actin-bundle turnover in neuronal growth cones. *Nat. Cell Biol.* 8:216–226.
64. Liu, A. C., and A. I. Gotlieb. 2007. Characterization of cell motility in single heart valve interstitial cells in vitro. *Histol. Histopathol.* 22: 873–882.
65. Applewhite, D. A., M. Barzik, S. I. Kojima, T. M. Svitkina, F. B. Gertler, and G. G. Borisy. 2007. Ena/VASP proteins have an anti-capping independent function in filopodia formation. *Mol. Biol. Cell.* 18:2579–2591.
66. Baas, A. F., J. Kuipers, N. N. van-der Wel, E. Batlle, H. K. Koerten, P. J. Peters, and H. C. Clevers. 2004. Complete polarization of single intestinal epithelial cells upon activation of LKB1 by STRAD. *Cell.* 116:457–466.
67. Runge, K. E., J. E. Evans, Z. Y. He, S. Gupta, K. L. McDonald, H. Stahlberg, P. Primakoff, and D. G. Myles. 2007. Oocyte CD9 is enriched on the microvillar membrane and required for normal microvillar shape and distribution. *Dev. Biol.* 304:317–325.
68. Mossman, K., and J. T. Groves. 2007. Micropatterned supported membranes as tools for quantitative studies of the immunological synapse. *Chem. Soc. Rev.* 36:46–54.
69. Harder, T., C. Rentero, T. Zech, and K. Gaus. 2007. Plasma membrane segregation during T cell activation: probing the order of domains. *Curr. Opin. Immunol.* 19:470–475.
70. Pokutta, S., and W. I. Weis. 2007. Structure and mechanism of cadherins and catenins in cell-cell contacts. *Annu. Rev. Cell Dev. Biol.* 23:237–261.
71. Chu, Y. S., W. A. Thomas, O. Eder, F. Pincet, E. Perez, J. P. Thiery, and S. Dufour. 2004. Force measurements in E-cadherin-mediated cell doublets reveal rapid adhesion strengthened by actin cytoskeleton remodeling through Rac and Cdc42. *J. Cell Biol.* 167: 1183–1194.
72. Weis, W. I., and W. J. Nelson. 2006. Re-solving the cadherin-catenin-actin conundrum. *J. Biol. Chem.* 281:35593–35597.
73. Weisswange, I., T. Bretschneider, and K. I. Anderson. 2005. The leading edge is a lipid diffusion barrier. *J. Cell Sci.* 118:4375–4380.
74. Guo, W. H., M. T. Frey, N. A. Burnham, and Y. L. Wang. 2006. Substrate rigidity regulates the formation and maintenance of tissues. *Biophys. J.* 90:2213–2220.
75. Goffin, J. M., P. Pittet, G. Csucs, J. W. Lussi, J. J. Meister, and B. Hinz. 2006. Focal adhesion size controls tension-dependent recruitment of α-smooth muscle actin to stress fibers. *J. Cell Biol.* 172: 259–268.
76. Cukierman, E., R. Pankov, D. R. Stevens, and K. M. Yamada. 2001. Taking cell-matrix adhesions to the third dimension. *Science.* 294: 1708–1712.
77. Hinz, B. 2006. Masters and servants of the force: the role of matrix adhesions in myofibroblast force perception and transmission. *Eur. J. Cell Biol.* 85:175–181.
78. Chen, C. S., J. L. Alonso, E. Ostuni, G. M. Whitesides, and D. E. Ingber. 2003. Cell shape provides global control of focal adhesion assembly. *Biochem. Biophys. Res. Commun.* 307:355–361.

79. Ingber, D. E. 2006. Cellular mechanotransduction: putting all the pieces together again. *FASEB J.* 20:811–827.

80. Paszek, M. J., N. Zahir, K. R. Johnson, J. N. Lakins, G. I. Rozenberg, A. Gefen, C. A. Reinhart-King, S. S. Margulies, M. Dembo, D. Boettiger, D. A. Hammer, and V. M. Weaver. 2005. Tensional homeostasis and the malignant phenotype. *Cancer Cell.* 8:241–254.

81. Lam, W. A., M. J. Rosenbluth, and D. A. Fletcher. 2007. Chemotherapy exposure increases leukemia cell stiffness. *Blood.* 109:3505–3508.

82. Sens, P., and S. A. Safran. 1998. Pore formation and area exchange in tense membranes. *Europhys. Lett.* 43:95–100.

83. Bohil, A. B., B. W. Robertson, and R. E. Cheney. 2006. Myosin-X is a molecular motor that functions in filopodia formation. *Proc. Natl. Acad. Sci. USA.* 103:12411–12416.